MODELING AND CHARACTERIZATION OF HONEYCOMB FRP SANDWICH BEAMS IN TORSION

Justin Robinson, WVU, Morgantown, WV
Julio F. Davalos, WVU, Morgantown, WV
Pizhong Qiao, U of Akron, Akron, OH

Abstract

Fiber reinforced plastic (FRP) cellular panels have been increasingly used in highway bridges, both in new construction and rehabilitation and replacement of existing bridge decks. Recent applications have demonstrated that honeycomb FRP panels can be effectively and economically used for highway bridge deck systems. However, their mechanical properties and behaviors have not been fully explored. Thus, the objective of this study is to conduct a combined experimental and analytical investigation of honeycomb FRP sandwich beams subjected independently to bending and torsion loads. The emphasis of this paper is on torsion experiments and finite element modeling. The sandwich panel considered in this study has a sinusoidal core geometry in the plane extending vertically between face laminates, as shown in Figure 1. The analyses of the honeycomb structure and components include: (1) constituent materials and ply properties, (2) face laminate and core wall engineering properties, and (3) equivalent core material properties. A homogenization process is used to obtain the equivalent core material properties for the honeycomb geometry with sinusoidal waves. Timosenko's beam theory combined with lamination theory is used to analyze the beams in bending, and finite element models of the test samples using layered shell elements are used to correlate results with bending analytical predictions and experimental results in bending and torsion. To verify the accuracy of the analytical and numerical solutions, several honeycomb sandwich beams with sinusoidal core waves either in the longitudinal or transverse directions are tested in bending and torsion. The present analysis and characterization procedures can be used in design applications and optimization of honeycomb structures and to obtain equivalent material properties of honeycomb FRP beams with several core geometries.

Keywords: Honeycomb FRP sandwich panel, Torsion, Finite element modeling

Introduction

While honeycomb structures are commonly used in the automotive and aerospace industries, there are only few applications in civil infrastructure. However, the recent fast growing interest in composite materials for the rehabilitation and new construction of bridge decks provides an excellent opportunity for development and implementation of honeycomb structures. In general, because of the relatively low stiffness of polymer composites (E-glass fibers and polymer resins), FRP structures usually exhibit large deformations, and therefore, their accurate response predictions under various loading conditions are important. In particular, honeycomb fiber-reinforced plastic (HFRP) structures have been successfully applied in bridge construction, but their mechanical properties have not been fully explored.

The concept of a lightweight and heavy-duty FRP panel with a sinusoidal core configuration in the plane extending vertically between face laminates (Figure 1) was introduced for highway bridge decks by Plunkett (1997). Since then, several other uses, including fish raceway tanks (Davalos et al.,

2002), have been explored. After evaluating the favorable characteristics of sandwich panels for bridge decks and other applications, several studies for testing and field installations were successfully completed. However, the design modeling and optimization of the HFRP structure was not rigorously undertaken, partially due to the complex core geometry. In this study, an overview of an approximate analytical solution verified by finite element modeling and experimental testing of beam samples in bending is presented, and a detailed examination of beam samples in torsion is given, based on finite element analyses and experimental evaluations.

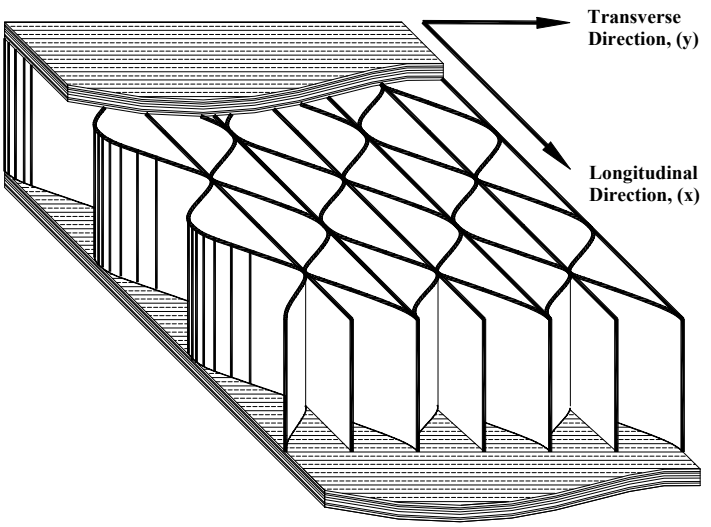

Figure 1. Configuration of Honeycomb FRP Sandwich Panel

Modeling Of Honeycomb FRP Sandwich Panel

In this section, the geometry and characteristics of the honeycomb FRP sandwich panel are presented. Equivalent properties of face laminates are obtained using micro/macromechanics models, while the effective orthotropic properties of the honeycomb core are obtained from a homogenization process using combined energy method and mechanics of materials approach (Davalos et al., 2001).

The HFRP panel considered in this study was developed by Kansas Structural Composites, Inc. (Plunkett, 1997), and the sandwich structure consists of two face laminated plates co-cured with a core of sinusoidal configuration (Figure 1). This core geometry was conceived to increase the stiffness and buckling capacity of the panel by continually supporting the face laminates with the core elements. The core geometry consists of closed honeycomb-type cells, formed by a repetitive combination of a flat component and a waved component, which is defined by a sinusoidal function (Figure 1). The waved component of the core is manufactured by forming FRP sheets into a corrugated mold. A plan view of the core is shown in Figure 2. For the samples used in this study, both the face and core laminates were produced from E-glass fibers and polyester resin, and the total thickness of the panel was approximately five inches.

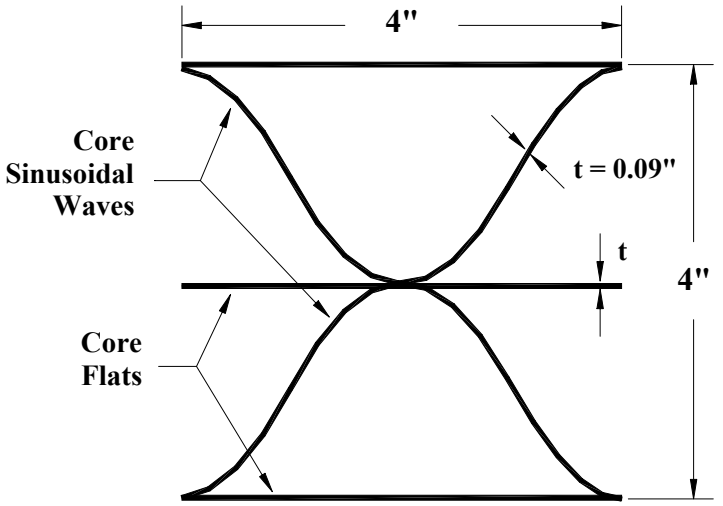

Figure 2. Plan View of Honeycomb Sinusoidal Core

Modeling of Face Laminates

The engineering properties for the face laminates are obtained from a micro/macromechanics approach. Using micromechanics, the stiffness properties of each layer, or ply, of the laminate can be predicted, and based on the ply properties and lay-up, the apparent stiffness of the laminate can be found using classical lamination theory (Davalos et al., 1996).

The fiber architecture of the top and bottom face laminates is symmetric about the mid-plane of the sandwich panel. Each face laminate includes the following types of layers: (1) a 0°/90° bi-directional stitched fabric (CM-3205) together with continuous strand mat (ContSM), (2) a unidirectional layer (UM-1810) and a ContSM, and (3) a chopped strand mat (ChSM) bonding layer at the interface of the core. The lay-up for the face laminate used in this study, starting at the interface, consists of one ChSM bond layer, a CM-3205/ContSM layer, six layers of the UM-1810/ContSM, and a final layer of CM-3205/ContSM. The total face panel thickness is approximately 0.43 inches. The layer stiffness values are summarized in Table 1, and further details can be found in Davalos et al. (2001) and Robinson et al. (2001).

Table 1. Layer Stiffness Properties

Ply type	Orientation	E_1,msi	E_2,msi	G_{12},msi	G_{23},msi	v_{12}	v_{23}
ChSM Bond Layer	Random	1.41	1.41	0.507	0.308	0.394	0.401
CM-3205	0˚/90˚	4.02	1.16	0.447	0.417	0.295	0.39
CSM[a]	Random	1.71	1.71	0.61	0.343	0.402	0.4
Um-1810	0˚	4.36	1.24	0.479	0.447	0.293	0.386
CSM[a]	Random	2.31	2.31	0.82	0.43	0.409	0.388

Note: *a* refers to CSM layer attached to previous fabric.

The equivalent elastic properties of the face laminates are computed from classical lamination theory. Using the ply properties found by micromechanics, a set of equivalent laminate properties (E_x, E_y, G_{xy}, v_{xy}) can be defined. These constants represent an equivalent orthotropic plate that behaves in the same manner as the actual laminate under in-plane loading. The equivalent elastic properties of the laminate are summarized in Table 2.

Table 2. Stiffness Properties Of Face Laminates

E_x, x10^6 psi	E_y, x10^6 psi	ν_{xy}	G_{xy}, x10^6 psi
2.846	1.850	0.302	0.546

Modeling of Honeycomb Core

The elastic equivalence analysis of the sinusoidal-waved honeycomb core structure (see Figures 1 and 2), as given by Davalos et al. (2001), is based on a homogenization concept combined with an energy method and a mechanics of materials approach. The homogenization process of the periodic core structure required defining a Representative Volume Element (RVE), for which the global properties were obtained by invoking periodic conditions and approximations. The honeycomb core was produced from ChSM, with a thickness of *t=0.09"* (see Figure 2), and its equivalent properties are given in Table 3, where the in-plane coordinates x-y are shown in Figure 1. While exact solutions are obtained for Young's moduli using mechanics of materials approach, the evaluation of shear stiffnesses usually involve complex analyses with upper and lower bounds derived from an energy method, but as shown in Table 3, the bounds for out-of-plane shear moduli are within a narrow range, and therefore, the lower bound can be conservatively used.

Table 3. Elastic Equivalent Properties For Honeycomb Core

Core wall properties: $E_1^s = E_2^s = 1.71 \times 10^6$ psi; $G_{12}^s = 0.611 \times 10^6$ psi			
Young's Moduli	E_x^e	E_y^e	E_z^e
	$0.0449\ E_1^s$	$8.36\text{x}10^{-5}\ E_1^s$	$0.107\ E_2^s$
Shear Moduli	G_{xy}^e	G_{xz}^e	G_{yz}^e
Upper bound	$5.98\text{x}10^{-5}\ E_1^s$	$0.078\ G_{12}^s$	$0.033\ G_{12}^s$
Lower bound	$5.98\text{x}10^{-5}\ E_1^s$	$0.075\ G_{12}^s$	$0.027\ G_{12}^s$
Poisson's Ratios	ν_{xy}^e	ν_{xz}^e	ν_{yz}^e
	0.431	0.169	$0.273\text{x}10^{-4}$

Note: *e* refers to quantities with equivalent properties;
s refers to quantities of core material properties.

Overview Of HFPR Beams In Bending

An overview of responses and predictions for HFRP beam samples in bending is presented in this section. Comparisons of finite element and analytical results with experimental evaluations are used to validate the equivalent material properties given in the preceding section. Tables 4 and 5 present comparisons of midspan deflections and tensile strains for longitudinal and transverse beam samples under three- and four-point bending. Further information and details about the bending study are given by Robinson et al. (2001), Davalos et al. (2001) and Robinson (2001).

The finite element and analytical predictions of displacements compare well with the experimental values, with the transverse samples showing smaller differences. The range of percent difference from experimental values for the longitudinal samples is between 6 to 20%, with the actual geometry finite element models showing smaller discrepancies. The transverse samples show a lower percentage difference from experimental deflection values, with a maximum difference of 10%. The predictions of the midspan tensile strains show larger percentage differences than those of the deflections. The most favorable predictions for the longitudinal samples were found using the actual geometry finite element model. However, for the transverse beams, each of the numerical and analytical models predicted the strains well.

Table 4. Comparison of Midspan Deflections for HFRP Beam Samples

Core Orientation	Span, feet	Width, inches	Bending Type	Deflection, in./kip						
				Exp.	FE Model				Analytical	
					Actual		Equivalent			
				@ 1/2 Span	@ 1/2 Span	% from Exp.	@ 1/2 Span	% from Exp.	@ 1/2 Span	% from Exp.
Longitudinal	15.0'	12"	3-point	0.684	0.701	2.5	0.788	15.2	0.753	10.1
			4-point	0.572	0.645	12.8	0.668	16.8	0.639	11.7
		8"	3-point	1	1.087	8.7	1.18	18.0	1.13	13.0
			4-point	0.836	0.921	10.2	1	19.6	0.958	14.6
	11.5'	12"	3-point	0.321	0.348	8.4	0.36	12.1	0.344	7.2
			4-point	0.263	0.294	11.8	0.305	16.0	0.291	10.6
		8"	3-point	0.466	0.498	6.9	0.541	16.1	0.517	10.9
			4-point	0.385	0.421	9.4	0.399	3.6	0.437	13.5
	8.0'	12"	3-point	0.115	0.122	6.1	0.126	9.6	0.12	4.3
			4-point	0.097	0.103	6.2	0.105	8.2	0.101	4.1
		8"	3-point	0.161	0.184	14.3	0.189	17.4	0.18	11.8
			4-point	0.136	0.155	14.0	0.158	16.2	0.151	11.0
	5.5'	12"	3-point	0.051	0.043	-15.7	0.044	-13.7	0.042	-17.6
		8"	3-point	0.061	0.065	6.6	0.066	8.2	0.063	3.3
Transverse	8.0'	12"	3-point	0.207	0.2	-3.4	0.223	7.7	0.202	-2.4
			4-point	0.176	0.167	-5.1	0.174	-1.1	0.169	-4.0
		8"	3-point	0.335	0.301	-10.1	0.315	-6.0	0.304	-9.3
			4-point	0.275	0.251	-8.7	0.262	-4.7	0.253	-8.0
	5.5'	12"	3-point	0.08	0.073	-8.8	0.081	1.3	0.073	-8.8
		8"	3-point	0.121	0.109	-9.9	0.115	-5.0	0.109	-9.9

Table 5. Comparison of Midspan Tensile Strains for HFRP Beam Samples

Core Orientation	Span, feet	Width, inches	Bending Type	Strain @ Midspan, microstrain/kip						
				Exp.	FE Models				Analytical	
					Actual		Equivalent			
				Strain	Strain	% from Exp.	Strain	% from Exp.	Strain	% from Exp.
Longitudinal	15.0'	12"	3-point	570	659	15.6	713	25.1	683	19.8
			4-point	373.5	435	16.5	475	27.2	455	21.8
		8"	3-point	836	964	15.3	1069	27.9	1024	22.5
			4-point	558	646	15.8	712	27.6	683	22.4
	11.5'	12"	3-point	438	507	15.8	546	24.7	524	19.6
			4-point	288	334	16.0	364	26.4	349	21.2
		8"	3-point	633	738	16.6	820	29.5	785	24.0
			4-point	425	495	16.5	546	28.5	524	23.3
	8.0'	12"	3-point	303	354	16.8	380	25.4	364	20.1
			4-point	200	233	16.5	253	26.5	243	21.5
		8"	3-point	439	513	16.9	571	30.1	546	24.4
			4-point	295	345	16.9	380	28.8	364	23.4
	5.5'	12"	3-point	209	245	17.2	261	24.9	250	19.6
		8"	3-point	298	352	18.1	393	31.9	376	26.2
Transverse	8.0'	12"	3-point	564	481	-14.7	641	13.7	595	5.5
			4-point	382	348	-8.9	403	5.5	397	3.9
		8"	3-point	881	833	-5.4	907	3.0	892	1.2
			4-point	570	567	-0.5	604	6.0	595	4.4
	5.5'	12"	3-point	386	318	-17.6	441	14.2	409	6.0
		8"	3-point	590	567	-3.9	624	5.8	614	4.1

A possible reason for the differences between experimental values and analytical and numerical predictions for the longitudinal samples may be due to discontinuities at the interface bond between the core and face sheets. Also, an examination of the data for the longitudinal samples leads us to conclude that the prediction of equivalent longitudinal out-of-plane shear stiffness needs further refinement. This problem plays a more significant role in the torsion responses, as discussed further in the following section.

Characterization Of HFRP Beams In Torsion

Analytical models are valuable for describing responses of the HFRP beam samples considered in this study. However, due to the complex geometry of the sandwich panel, a closed-form solution for torsion is not available at this time. Thus, an experimental study is presented, supplemented by a finite element analysis to evaluate the response of the samples in torsion.

Experimental Study

Experimental testing of beam samples is conducted to verify finite element results. Longitudinal and transverse samples are instrumented and loaded in torsion, as described below. The machine used to experimentally test samples in torsion was designed by a former graduate student at West Virginia University, who provided design details in his thesis (Brokaw, 1992). A diagram of the torsion machine

is shown in Figure 3. To esttablish confidence on the accuracy of the experimental results, the torsion machine was fist calibrated using an aluminum bar.

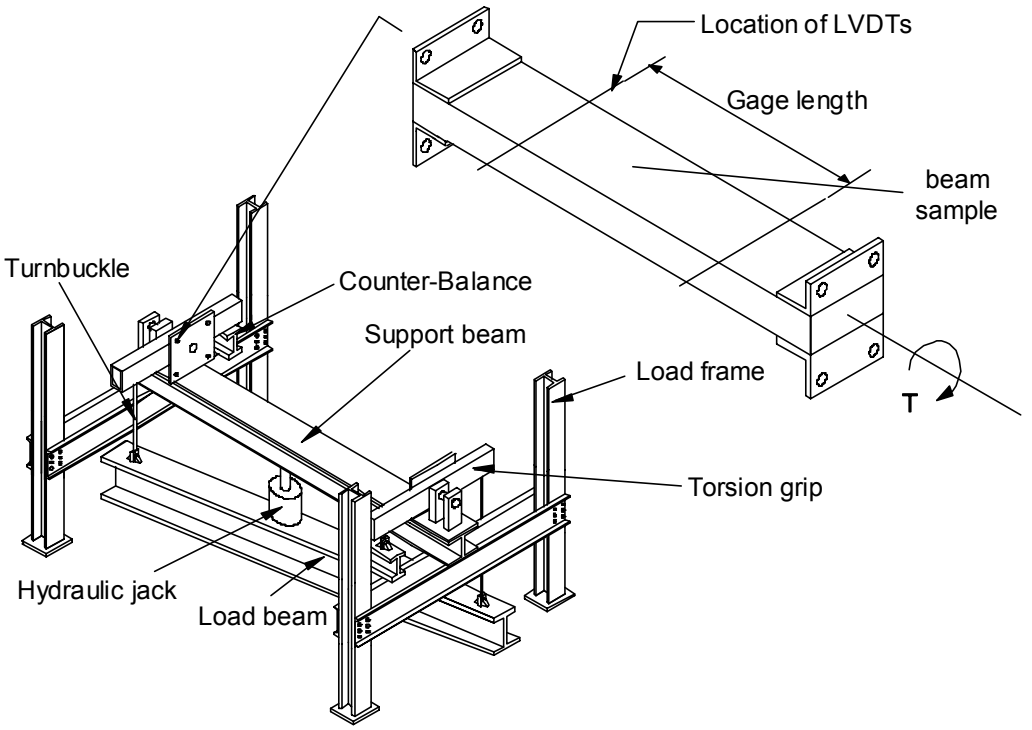

Figure 3. Torsion Machine

The calibration of the machine had two objectives: (1) to experimentally measure the angle of rotation and predict its value from St. Venant's solution, using the applied torque and published shear modulus; and (2) to create a finite element model of the aluminum bar and compare its responses with the experimental results for angle of rotation. The angle of rotation results for the aluminum bar at the gauge length of L = 36" are given in Table 6, where the percent differences between the analytical and finite element predictions with the average experimental result are, respectively, 7.5% and 2.7%. These small percent differences provided confidence to proceed with the FE modeling and the experimental testing of the HFRP samples.

.

Table 6. Summary of Angle of Rotation for the Aluminum Bar

	Analytical Prediction	**Finite Element Prediction**	**Experimental Results, Average**
Angle of Rotation, radians/kip-in	0.00475	0.00442	0.00454

The samples used in the experimental evaluation include three with longitudinal core orientation (one 12-inch wide and two 8-inches wide) that are ten feet long, and four with transverse core orientation (two 12-inches wide and two 8-inches wide) that are nine feet long. The beams are instrumented with two shear strain gages (±45° to record shear strain) and with four linear voltage differential transducers (LVDT's), which are used to determine angle of rotation. Two LVDT's are placed on each side of the beam at a distance of 3-feet from the midspan in the direction of the end-

support, and each of the two LVDT's is suspended from a rod extending 24 inches normal to the beam as shown in Figure 4. The torque is applied to the sample by a hydraulic jack, which applies a force to the load beam, against the reaction at the support beam (Figure 3). The load is transferred diagonally to the turnbuckles, which in turn, cause the ends of the beam sample to rotate opposite to each other. Ideally, the center of the beam sample would have absolutely no rotation, thus simulating a fixed boundary condition at the midspan. The recorded values are load and deflections, which are then converted to applied torque and induced angle of rotation, respectively.

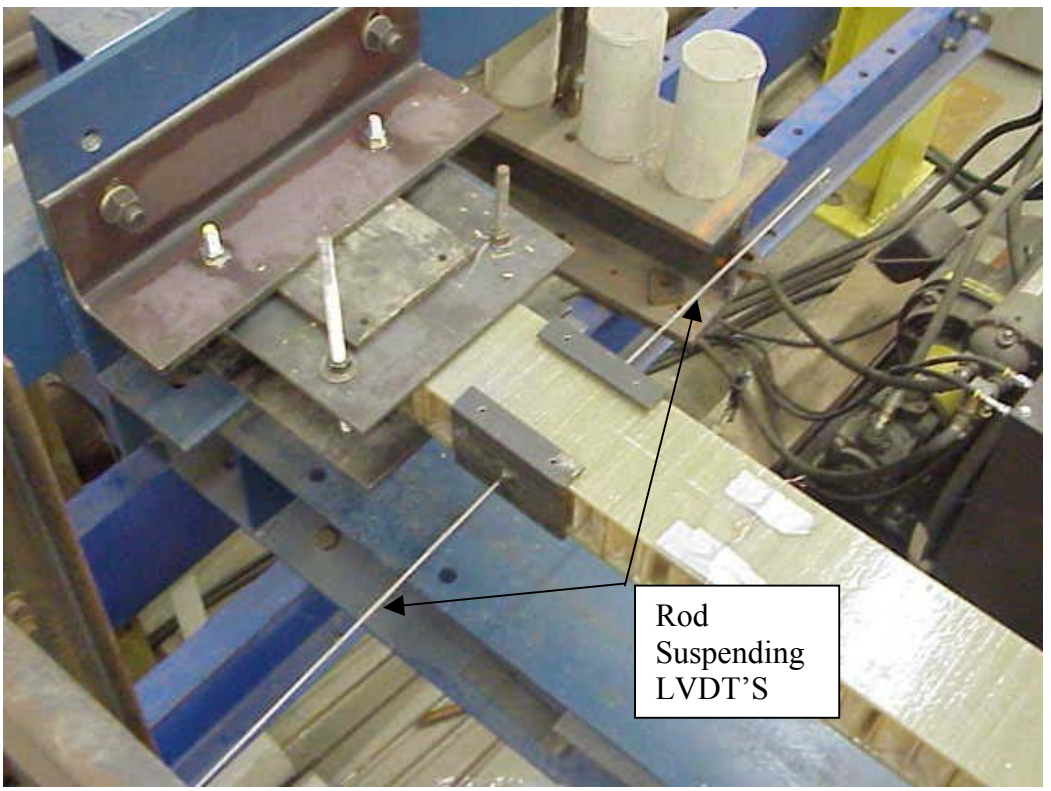

Figure 4. Experimental Arrangement for HFRP Beam Samples in Torsion

Experimental values of angle of rotation are given in Table 7, where each result is obtained from the tangent of the average angle, which found by taking the average of the absolute values of the four deflections (two at each end) and dividing that number by the distance between the center width of the beam and the end of the rod holding the LVDT core (Figure 4). Results are given in radians per kip-inch. Shear strain values are shown in Table 8 as micro strains per kip-inch.

Finite Element Modeling

Finite element analyses are performed to predict the responses of the several beam samples used in the experimental study. The results are then compared with the experimental values. As with the beams in bending, there are two types of models produced for examination. The actual geometry models are created with appropriate core orientations and sample widths using layered shell elements to replicate the actual geometry of the samples. The length of each model is three feet, which is one-half of the gauge length used in the experimental testing. A fixed-free boundary condition is assumed in the model, with all of the nodes at one end completely constrained, while only the center node at the other end is prevented to translate normal to the geometric cross-sectional axis. This is to prevent out-of-

plane bending. The torque is applied using a coupled traction loading on the top and bottom edge nodes of the free end of the model. The amount of torque applied is 1 kip-inch. The shear strain data can be obtained at the point of interest by simply examining the nodal average of the strains. However, the task of finding the angle of rotation is not so simple. The lateral displacements in the width direction of the center nodes of the top and bottom plates can be used to define a right triangle, and using small-angle theory, the sum of their displacements can be divided by their vertical distance to give the angle of twist (Robinson, 2001). The values of interest are given in tables 7 and 8. A displacement contour of a typical actual geometry model is given in Figure 5.

The FE equivalent plate model consists of 3-layer shell elements with material properties defined by the equivalent orthotropic values. The overall dimensions of the models are the same with respect to the actual geometry models, and the same fixed-free boundary condition is used, with the center node at the free-end constrained against out-of-plane translations. A torque of 1 kip-inch is applied by using two coupled, nodal loads at opposite edges of the free end. The angle of rotation and shear strains of interest can be directly obtained from the model at the location of interest. The values of interest are also given in tables 7 and 8.

Discussion of Torsion Results

The comparisons for the longitudinal samples show large percent differences between the finite element models and experimental results. There are several possible reasons for this discrepancy. First, it could be due to testing inaccuracies. The torsion test procedure is difficult to implement, and any small errors could influence the results greatly. Second, the observed lack of consistency in the manufacturing quality of the samples probably affected the testing results. A serious problem that was observed during the torsion tests was some delamination of the face-sheet from the core. This problem was particularly evident for the 12-inch wide and #2 8-inch wide longitudinal samples; thus the measured torsional responses for these samples are likely to be in error with respect to the FE results.

Another possible source of error in the analysis could be the inaccuracy of the longitudinal out-of-plane shear stiffness. As can be seen in Table 7, the actual and equivalent-plate finite element models for the longitudinal samples predict stiffer responses than experimentally measured, while for the transverse samples the percent differences are reasonable.

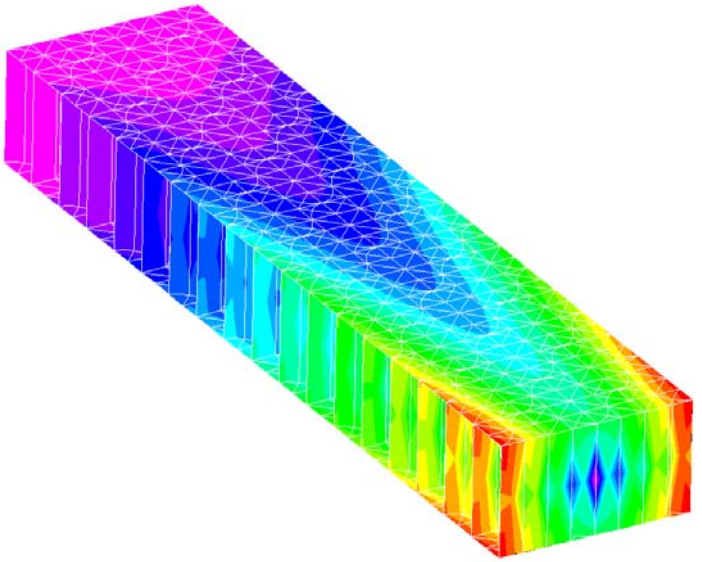

Figure 5. Displacement Contour for 8" Transverse Sample in Torsion

Table 7. Comparison of FE and Experimental Values of Angles of Rotation

Core Orientation	Width	Sample	Angle of Rotation, radians/kip-in			% Difference of FE Actual and FE Equivalent	% Difference of Exp. and FE Actual
			FE Actual	FE Equiv.	Exp.		
Longitudinal	12"	#1	0.0007	0.0006	0.001	-14.3	-30.0
	8"	#1	0.0016	0.0013	0.00174	-18.8	-8.0
		#2			0.00121		32.2
Transverse	12"	#1	0.0009	0.001	0.00098	11.1	-8.2
		#2			0.00111		-18.9
	8"	#1	0.0026	0.0028	0.00306	7.7	-15.0
		#2			0.0031		-16.1

Table 8. Comparison of FE and Experimental Values of Shear Strains

Core Orientation	Width	Sample	Shear Strain, microstrain/kip-in.				% Difference of FE Actual and FE Equiv.	% Difference of Exp. and FE Actual	
			FE Model		Experimental				
			Actual	Equiv.	#1	#2		#1	#2
Longitudinal	12"	#1	44	68	47	50	54.5	6.8	13.6
	8"	#1	66	102	66	70	54.5	0	6.1
		#2			81	71		22.7	7.6
Transverse	12"	#1	58	67	55	58	15.5	-5.5	0
		#2			65	61		12.1	5.2
	8"	#1	96	103	83	99	7.3	-15.7	3.1
		#2			100	89		4.2	-7.9

In general, it is a difficult task to obtain shear strain values at a point from the FE results, due to the complexity of the geometry, but it can be seen from Table 8 that the actual FE models provide better correlations with experimental values than the equivalent-plate models. With the exception of the #1 8-inch wide longitudinal sample, relatively small percent differences are found between the actual FE models and the experimental results. However, the equivalent-plate FE models show larger percent differences, especially for the longitudinal samples. Again, this could be due to either manufacturing irregularities or inaccurate estimations of the longitudinal out-of-plane shear stiffness properties.

The quality of manufacturing has an important role in developing integral bond between the top and/or bottom face plates and the core, and the strength of the interface bond is much more critical for a torsion loading condition. It was noticed that some delamination between the core and face plates had occurred prior to as well as during the torsional loading. This delamination could cause the torsional stiffness to decrease. However, the finite element model assumes a perfect contact between core and face plates, and thus gives a higher stiffness.

It should also be noted that during bending, the shear effects are small. Even if some portion of the core had delaminated from the face plates, the top and bottom face plates, which act as beam flanges, are still held at the same locations away from the neutral axis, thus still effectively carrying the bending moment. In contrast, during torsional loading of the HFRP sandwich beams, the dominant properties that influence torsional rigidity are the in-plane and out-of-plane shear stiffnesses which are quite sensitive to delamination effects.

Conclusion

We present in this paper a combined analytical and experimental characterization of honeycomb fiber-reinforced plastic beams under bending and torsion, with emphasis on experimental procedures and numerical modeling for torsional loading. The core consists of in-plane sinusoidal cells extending vertically between top and bottom face laminates. While the experimental results correlate reasonably well with finite element predictions, refinements in manufacturing quality and predictions of equivalent out-of-plane shear stiffness properties could increase the accuracy of the correlations. Thus, a further study of shear effects by a closed-form solution and using better estimates of shear moduli properties is a topic of further research by the present authors.

Acknowledgement

The test samples were generously provided by Kansas Structural Composites Inc. (KSCI), and we thank the KSCI's President Dr. Jerry Plunkett for his technical contributions. Partial financial support for this study was provided by the NCHRP-IDEA program, National Academy of Sciences; and the NSF Partnerships for Innovation Program.

References

1. Brokaw, J.T. 1992. *Test methods to determine strength and stiffness properties for stress-laminated timber bridge decks.* M.S. Thesis, West Virginia University, Morgantown, WV.
2. Davalos, J.F., Qiao, P.Z., Xu, X.F., Robinson, J. and Barth, K.E. 2001. "Modeling and characterization of fiber-reinforced plastic honeycomb sandwich panels for highway bridge applications," *J. Comp. Struct.* 52(2001): 441-452.
3. Davalos, J.F., Robinson, J., Vantaram, A., Viadero, R.C., Semmens, K., Plunkett, J.D., 2002. "Honeycomb Fiber Reinforced Polymer Sandwich Panels for Fish Culture Tanks," *Proceedings of the 3rd International Conference on Composites in Infrastructure (ICCI'02)*, San Francisco, CA, June 10-12 (In press).
4. Davalos, J. F., Salim, H. A., Qiao, P.Z., Lopez-Aide, R. and Barbero, E. J. 1996. "Analysis and design of pultruded FRP shapes under bending," *Composites: Part B, Engineering J*., 27(3-4): 295-305.
5. Plunkett, J.D. November 1997. "Fiber-reinforced polymer honeycomb short span bridge for rapid installation," NCHRP-IDEA Project Report.
6. Robinson, J. 2001. *Analytical and experimental study of FRP honeycomb sandwich panels with sinusoidal core.* M.S. Thesis, West Virginia University, Morgantown, WV.
7. Robinson, J., Davalos, J.F., Xu, X.F., Qiao, P.Z., and Barth, K.E. 2001. "FRP honeycomb composite sandwich beams under bending," *Proceedings of the ASC 16th Annual Technical Conference, American Society of Composites (ASC),* Blacksburg, VA, Sept. 9-12 (in CD-ROM, Paper#111, 12 pages).